Split Resistor Synergetic MPPT algorithm for High-Altitude Solar-Powered UAVs

Saranya Mukherjee
Institute of Radiophysics and Electronics
University of Calcutta
Kolkata, India
ORCID: 0009-0004-3408-0341

Subhojoy Pal
Institute of Radiophysics and Electronics
University of Calcutta
Kolkata, India
ORCID: 0009-0001-8118-3278

***Abstract*—High-Altitude Long Endurance (HALE) Unmanned Aerial Vehicles (UAVs) rely on photovoltaic (PV) energy to sustain continuous operations, demanding lightweight and efficient power management. Extracting maximum solar power under rapidly changing irradiance and noisy sensor conditions remains challenging, as conventional Maximum Power Point Tracking (MPPT) algorithms either converge slowly, oscillate around the maximum power point, or impose high computational cost. Intelligent techniques such as fuzzy logic, artificial neural networks (ANN), and synergetic control improve performance, but none alone balances robustness, speed, and efficiency for aerospace applications. To address this gap, we propose a hybrid MPPT strategy improving on synergetic control, taking into account the system dynamics that a buck converter introduces, along with the fast, stable convergence of synergetic dynamics. Simulation results demonstrate that the proposed controller achieves near-99% tracking efficiency with convergence in 0.03 s and minimal steady-state oscillation. Furthermore, the system maintains almost full performance until the signal-to-noise ratio (SNR) of input measurements falls to 18 dB, highlighting its robustness in noisy environments. These results confirm the suitability of the proposed algorithm for real-world HALE UAV missions where efficiency, weight, and reliability are critical.**

***Index Terms*—Maximum Power Point Tracking (MPPT), Synergetic Control, Buck Converter, Hybrid Control, Photovoltaic Systems, High-Altitude Long Endurance (HALE) UAV.**

I. Introduction

Solar photovoltaic (PV) energy is essential for high-altitude long endurance (HALE) unmanned aerial vehicles (UAVs) to maintain continuous operations at stratospheric altitudes. Maximum power point tracking (MPPT) is a crucial subsystem for optimizing energy harvesting in situations with rapidly fluctuating temperature and irradiance. However, lightweight and effective MPPT algorithms are required due to the strict weight, power consumption, and onboard computational capacity restrictions of HALE UAVs [1]–[3].

Because of their simplicity, traditional MPPT algorithms like incremental conductance (IC) and perturb and observe (P&O) are still widely used [4]. However, these methods have serious shortcomings: While IC requires more computational work and still has trouble in dynamic conditions, P&O suffers from steady-state oscillations and is not very adaptable to sudden changes in irradiance [5].

To address these limitations, advanced MPPT techniques utilizing fuzzy logic, artificial neural networks, and swarm optimization have been investigated. Fuzzy logic controllers [6], [7] utilize rule-based systems to adaptively modify the output, ensuring robustness and modelling nonlinearity. However, they tend to fluctuate around the MPP, resulting in a loss of power and efficiency. Artificial neural networks (ANN) [8], [9] model nonlinear PV characteristics through feed-forward nets, achieving high accuracy but at the cost of significant computational cost at runtime. Swarm intelligence methods like particle swarm optimization (PSO) and ant colony optimization (ACO) [10]–[12] use bio-inspired global maximum tracking by iterative adjustment based on collective behavior. This offers both high accuracy and adaptability, but their iterative nature leads to very slow convergence times and thus lower efficiency. More intelligent algorithms like ACO inspired fuzzy logic systems [12] address the oscillation issue of fuzzy systems and sluggishness of ACO, but are computationally very intensive.

Alternatively, fractional order PID controllers [13], [14] use non-integer order integrals and differencials to model extreme non-linerarities and provide improved tracking but their range of linearity is limited. Synergetic control theory (SCT) [15]–[17] has recently emerged as a promising approach, delivering rapid convergence and low steady-state oscillations by enforcing system dynamics onto a convergent manifold. However, SCT may deviate from the exact MPP under certain conditions, especially when subject to buck converter configurations.

While each algorithm has their unique strengths, none alone fully satisfies the dual requirements of robustness and computational efficiency essential for HALE UAV missions. In our proposed algorithm, integrating fuzzy logic with synergetic control offers the potential to merge fuzzy adaptability with the dynamic stability of SCT, yielding a solution that is both efficient and lightweight for aerospace applications.

Table I summarizes the performance of representative MPPT methods in terms of convergence time, oscillation, and efficiency. Conventional and intelligent approaches address individual drawbacks but seldom achieve all three goals simultaneously. In contrast, the proposed hybrid Fuzzy-SCT method ensures fast tracking, low oscillations, and high efficiency with low computational cost.

This paper is structured as follows. Section VI-A, details the solar cell model used for simulation. Sections **??** and

TABLE I: Comparative performance of MPPT algorithms from recent literature

Reference/Year	Method	MPPT Time	Steady-State Oscillation	Efficiency
[12]/2024	ACO based Fuzzy Logic	≈ 0.88 s	$\pm 1.0\%$	$\approx 98.6\%$
[9]/2023	Artificial neural network (ANN)	≈ 0.03 s	$\pm 0.7\%$	$> 90\%$
[11]/2022	Particle swarm optimization (PSO)	> 1.0 s	$\pm 1.6\%$	$\approx 97.0\%$
[18]/2024	ANN with incremental conductance(IC)	≈ 0.066	$\pm 0.4\%$	$> 90\%$
[15]/2025	Synergetic Control Theory (SCT)	$\approx 0.03s$	$\pm 0.1\%$	$\approx 98.1\%$
proposed work	Split Resistor Synergetic Control	≈ 0.02 s	$\pm 0.087\%$	$\approx 98.94\%$

IV describe the individual fuzzy logic and synergetic control MPPT algorithms. Section **??** presents the proposed hybrid FLC+SCT MPPT strategy. Section VI discusses the simulation results, and Section VII concludes the paper.

II. Switching device modelling

The switch in the power converter block is practically implemented as a gate-driven MOSFET(Fig. 1a operated in the linear region or triode region. For the sake of analysis, we have assumed the device to be a long channel, uniformly doped, planar bulk NMOS transistor.

A pulse width modulated (PWM) voltage signal (V_{PWM}) controls the turning ON and turning OFF of the MOSFET. For the MOSFET to be ON, $V_{GS} \geq V_{TH}$ where V_{GS} refers to the gate-to-source voltage and V_{TH} refers to the threshold voltage of the MOSFET. Typically for discrete components, V_{GS} is of the order of a few volts. Hence, for the MOSFET to be ON,

$$V_{PWM} \geq V_S + V_{TH} \tag{1}$$

Once ON, for the MOSFET to be pushed into the linear region of operation,

$$0 \leq V_{DS} \leq V_{GS} - V_{TH} \implies V_D \leq V_{PWM} - V_{TH} \tag{2}$$

where V_{DS} refers to the drain-to-source voltage of the MOSFET.

In the linear region, the drain-to-source current flowing through the MOSFET is given by -

$$I = \mu_n C_{\text{ox}} \frac{W}{L} \left[(V_{GS} - V_{TH}) V_{DS} - \frac{V_{DS}^2}{2} \right] \tag{3}$$

Differentiating w.r.t. V_{DS},

$$\frac{\partial I}{\partial V_{DS}} = \mu_n C_{\text{ox}} \frac{W}{L} \left[(V_{GS} - V_{TH}) - V_{DS} \right] \tag{4}$$

So, in the ON state in the linear region, the MOSFET can be modelled as a voltage-controlled resistor R_{on}.

$$R_{on} = \left(\frac{\partial V_{DS}}{\partial I} \right) = \frac{1}{\mu_n C_{\text{ox}} \frac{W}{L} \left(V_{\text{PWM}} - V_D - V_{TH} \right)} \tag{5}$$

The following section uses this R_{on} to modify the buck converter state space equations to better reflect the switching device dynamics.

III. Split Resistor Buck Converter Model

As seen in the previous section, the switching element, ie, the MOSFET adds a series resistance only in the ON cycle of its operation. So, the traditional duty cycle averaged form of buck converter dynamics will not apply here.

Fig. 1 shows the effective on and off conditions of the buck converter configurations considering the R_{ON} introduced by the MOSFET.

A. ON state

In Fig. 1a, the conditions are as follows: input voltage V_g, inductor L, capacitor C, output/load resistance R, and a series resistance R_{on} that appears only in the ON state. The diode is ideal, and Continuous conduction mode (CCM) is assumed so the inductor current never reaches zero during switching. KVL around the inductor loop gives,

$$V_g - R_s i_L - L\dot{i}_L - v_C = 0$$

Rearrange to get the inductor differential equation:

$$\dot{I}_L = -\frac{R_{on}}{L} I_L - \frac{1}{L} V_C + \frac{1}{L} V_g. \tag{6}$$

The capacitor current is the difference between inductor current and load current:

$$I_C = I_L - \frac{C_C}{R}$$

so,

$$\dot{V}_C = \frac{1}{C} \left(I_L - \frac{V_C}{R} \right). \tag{7}$$

Write Eqn. (6) and (7) in matrix form $\dot{x} = A_1 x + B_1 V_g$:

$$A_1 = \begin{bmatrix} -\frac{R_s}{L} & -\frac{1}{L} \\ \frac{1}{C} & -\frac{1}{RC} \end{bmatrix}, \qquad B_1 = \begin{bmatrix} \frac{1}{L} \\ 0 \end{bmatrix}.$$

B. OFF state

In the OFF state(Fig. 1b the inductor directly discharges into the output node; KVL around the inductor loop gives

$$-L\dot{I}_L - V_C = 0$$

so,

$$\dot{I}_L = -\frac{1}{L} V_C \tag{8}$$

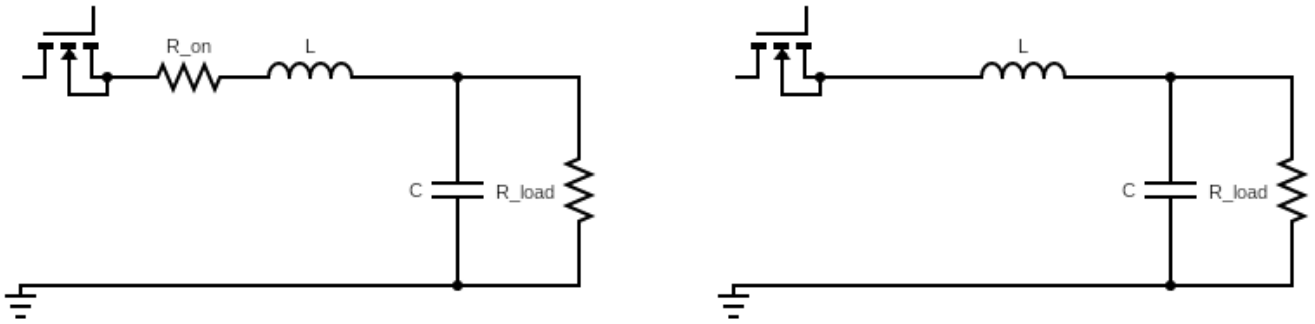

(a) Effective ON condition

(b) Effective OFF condition

Fig. 1: Buck converter ON and OFF conditions

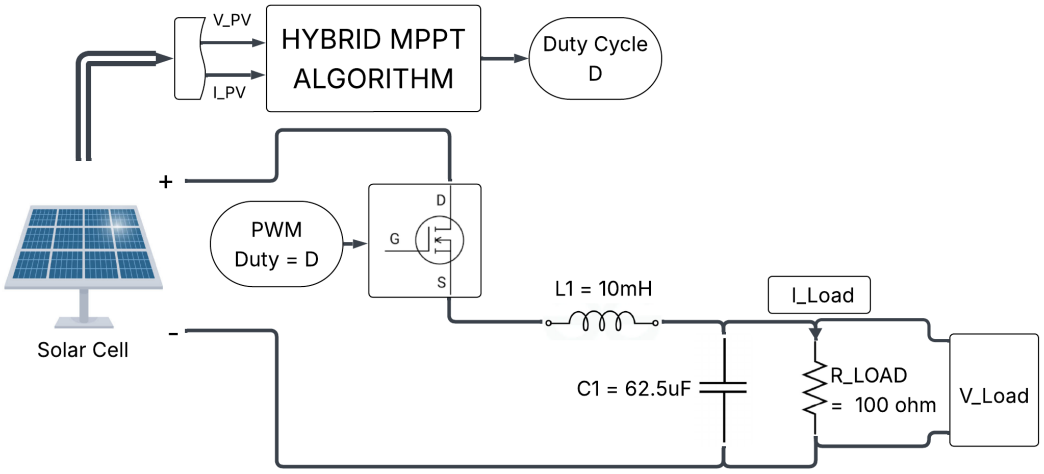

Fig. 2: Buck converter-based MPPT system architecture

The capacitor current equation is unchanged:

$$\dot{V}_C = \frac{1}{C}\left(I_L - \frac{V_C}{R}\right). \tag{9}$$

Matrix form $\dot{x} = A_2 x + B_2 V_g$ is

$$A_2 = \begin{bmatrix} 0 & -\frac{1}{L} \\ \frac{1}{C} & -\frac{1}{RC} \end{bmatrix}, \qquad B_2 = \begin{bmatrix} 0 \\ 0 \end{bmatrix}.$$

C. PWM based averaging

Over one cycle, the converter spends a fraction d in the ON state and $1-d$ in the OFF state(d is the duty cycle). By standard PWM averaging (assuming the switching frequency is much higher than the dynamics of interest), the averaged state matrices are,

$$\bar{A} = dA_1 + (1-d)A_2$$

$$\bar{B} = dB_1 + (1-d)B_2 = dB_1$$

Solving the averaged model,

$$\bar{A} = \begin{bmatrix} -\frac{dR_{on}}{L} & -\frac{1}{L} \\ \frac{1}{C} & -\frac{1}{RC} \end{bmatrix}, \qquad \bar{B} = \begin{bmatrix} \frac{d}{L} \\ 0 \end{bmatrix}.$$

The averaged state-space model is

$$\dot{x} = \begin{bmatrix} -\frac{dR_{on}}{L} & -\frac{1}{L} \\ \frac{1}{C} & -\frac{1}{RC} \end{bmatrix} x + \begin{bmatrix} \frac{d}{L} \\ 0 \end{bmatrix} V_g \tag{10}$$

or,

$$\dot{I}_L = \frac{1}{L}\left[-dR_{on} - V_C + dV_g\right] \tag{11}$$

$$\dot{V}_C = \frac{1}{C}\left(I_L - \frac{V_C}{R}\right) \tag{12}$$

IV. Synergetic Control Theory (SCT) for Buck Converters

Synergetic control is a nonlinear control methodology [15] based on the theory of dynamical system decomposition and

manifold enforcement. In MPPT applications, it allows for the creation of a global, converging control law without requiring full dynamic modeling. To derive the required control law, we need the system dynamics. We have derived our split resistor buck converter model in Eqn. 11,12. Then define a macro-variable:

$$\psi = \frac{dP_{pv}}{dI_{pv}} \tag{13}$$

The control law is designed [15] to ensure that ψ converges to the MPP value, which is defined as:

$$T\dot{\psi} + \theta(\psi) = 0 \tag{14}$$

Where T is a designer-chosen parameter that determines the rate of convergence to the invariant manifold $\psi(x,t) = 0$ specified by the macro-variable ψ. $\theta(\psi)$ is defined as a smooth differentiable function of that has to be selected, such that

- invertible and differentiable
- $\theta(0) = 0$
- $\theta(\psi)\psi > 0 \ \forall \psi \neq 0$

With these constraints, the $\theta(\psi)$ function can be chosen as:

$$\theta(\psi) = \psi(x,t) \tag{15}$$

So, we can define the invariant manifold as

$$\phi = \frac{\partial P_{pv}}{\partial I_{pv}} = 0 \tag{16}$$

Hence, assuming that $I_{pv} \approx I_L$,

$$\frac{\partial V_{pv} I_L}{\partial I_L} = I_L \frac{\partial V_{pv}}{\partial I_L} + V_{pv} = 0 \tag{17}$$

Now, combining Eqn. 11($V_g = V_{in}$) and 17,

$$\left(2\frac{\partial V_{pv}}{\partial I_L} + I_L \frac{\partial^2 V_{pv}}{\partial I_L^2}\right) \cdot \frac{1}{L}\left(-dR_{on} - V_C + dV_{in}\right) = -\frac{1}{T}\left(V_{pv} + I_L \frac{\partial V_{pv}}{\partial I_L}\right) \tag{18}$$

Using these equations a custom control law has been derived for the buck converter setup as follows:

$$d = \left[V_C - \frac{L}{T} \frac{V_{pv} + \frac{I_L \partial V_{pv}}{\partial I_L}}{2\frac{\partial V_{pv}}{\partial I_L} + I_L \frac{\partial^2 V_{pv}}{\partial I_L^2}}\right] \cdot \frac{1}{V_{in} - R_{on} I_L} \tag{19}$$

After optimisation, the control law converges to the MPP with a guaranteed stability margin (T = 0.0005).

V. Output Conditioning

In order to mitigate high-frequency switching noise and jitter at steady state, a low-pass FIR filter is applied to the duty cycle. Let $D_f[k]$ denote the filtered duty cycle sequence and $D[k]$ denote the updated duty cycle sequence. A length-M FIR low-pass filter with Dolph-Chebyshev window is defined as

$$h[n] \ = \ h_d[n] \ w[n], \qquad n = 0, \ldots, M-1 \tag{20}$$

where the ideal low-pass response is

$$h_d[n] \ = \ \begin{cases} \dfrac{\omega_c}{\pi}, & n = m_0, \\ \dfrac{\sin\big(\omega_c(n-m_0)\big)}{\pi(n-m_0)}, & n \neq m_0, \end{cases}$$

with $m_0 = (M-1)/2$. The Dolph-Chebyshev window is

$$w[n] \ = \ \frac{T_{M-1}\Big(\beta \cos\frac{\pi(n-m_0)}{M-1}\Big)}{T_{M-1}(\beta)} \tag{21}$$

where $T_{M-1}(\cdot)$ is the Chebyshev polynomial of order $M-1$. The parameters are

$$\omega_c = 2\pi\frac{f_c}{f_s}, \qquad \beta = \cosh\Big(\tfrac{1}{M-1}\operatorname{arccosh}(10^{A/20})\Big) \tag{22}$$

with f_c the cutoff frequency, f_s the sampling frequency, and A the sidelobe attenuation (dB). Finally, the filtered duty cycle is

$$D_f[k] \ = \ \sum_{m=0}^{M-1} h[m] \ D[k-m] \tag{23}$$

f_c and A are chosen to balance noise rejection with response time to give optimal performance at 2kHz and 50dB, respectively.

VI. Results and Discussion

A. Solar Cell Model

The photovoltaic source that is used for the simulation is represented using the single-diode model, which captures the nonlinear current-voltage characteristics of a solar cell. The output power P_{pv} is given by the equation:

$$P = n_p I_{pv} V - n_p I_0 \left(\exp\left(K_o\left(\frac{V}{n_s} + I_T R_{sT}\right)\right) - 1\right) V - \left(\frac{V}{n_s} + I_T R_{sT}\right)\frac{V}{R_{shT}} \tag{24}$$

Where:

- P_{pv} is the output power
- V is the output voltage
- I_{pv} is the output current proportional to input irradiance
- I_T is the output current proportional to the temperature
- I_o is the reverse saturation current of the panel
- K_o is the diode ideality factor
- I_T is the thermal voltage
- R_{sT} is the series resistance
- R_{shT} is the shunt resistance
- n_s is the number of series
- n_p is the number of parallel cells

Equation (24) ensures that the I-V and P-V curves under varying irradiance and temperature conditions are realistically reproduced, allowing for meaningful comparison of tracking behaviours. A standard thin-film solar cell designed for space applications, made by SHARP is chosen (Table II).

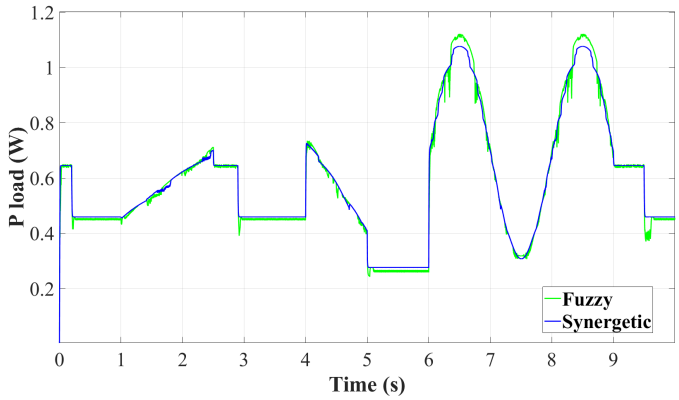

(a) Irradiance tracking of FLC and SCT algorithms

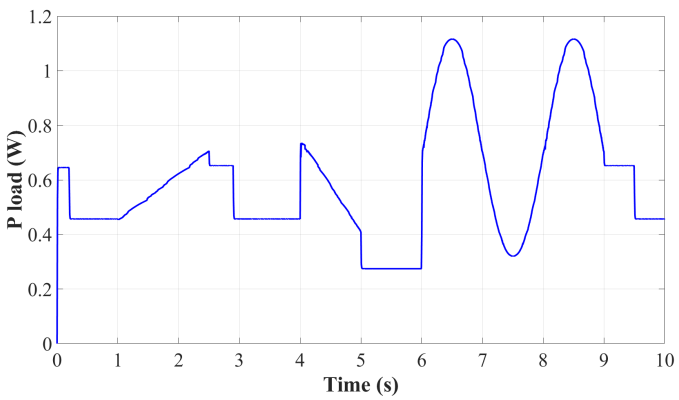

(b) Irradiance tracking of proposed algorithm

Fig. 3: MPPT algorithm irradiance tracking curves

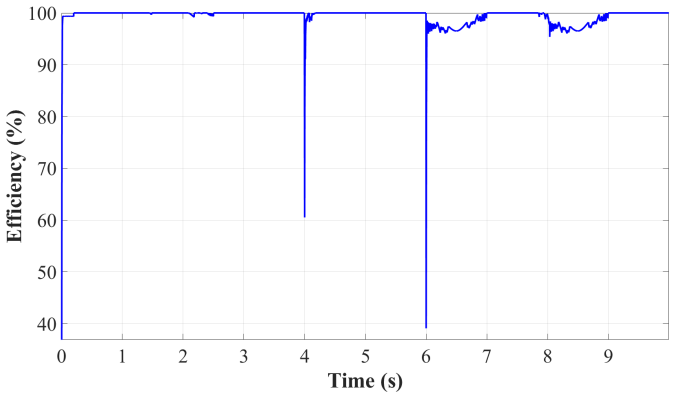

(a) Proposed algorithm's efficiency curve with no added noise

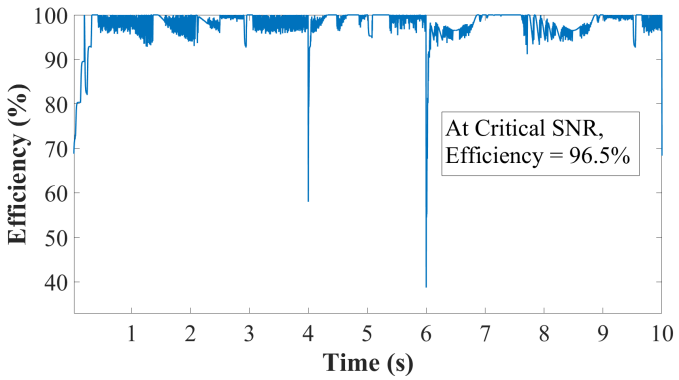

(b) Proposed algorithm's efficiency curve at critical SNR

Fig. 4: FLC + SCT hybrid efficiency curves

TABLE II: Solar Cell Parameters

Parameter	Value
I_{sc} (Short Circuit Current)	0.45 A
V_{oc} (Open Circuit Voltage)	3.05 V
I_{mpp} (MPP Current)	0.435 A
V_{pv} (MPP Voltage)	2.67 V
n_s (Number of Series Cells)	5
n_p (Number of Parallel Cells)	3

TABLE III: Comparison of hybrid MPPT algorithms

Algorithm	Efficiency	Convergence Time (s)	Steady-State Oscillations
proposed	98.94%	0.021s	0.087%
ANN + FOPID [19]	98.1%	0.049s	0.386%
ANN + SMC [20]	96.2%	0.22s	–
FOPID [13]	97.96%	0.03s	0.7%

B. Evaluation metrics

In order to evaluate the quality and practicality of each MPPT method, the subsequent metrics are recorded:

- **Efficiency:** Ratio of extracted power to the theoretical maximum available. Fig 5 shows the irradiance profile used for efficiency comparisons.
- **Convergence Time:** Time taken to reach the maximum power point under changing conditions. It is measured as the time taken by the algorithm to reach 95% of the MPP from 5%.
- **Steady-State Oscillation:** Steady-state fluctuations around the MPP expressed as a percentage of the MPP. More the steady-state oscillations, more the power loss.
- **Robustness:** The minimum SNR of the input V and I signals that the algorithm can process without losing more than 2% of its noise-free baseline characterises its behaviour under noise or disturbances. In real-world scenarios, where measurement noise is unavoidable, this metric shows how well the algorithm maintains dependable MPPT. (Lower SNR $\Longrightarrow$ Better noise tolerance.)

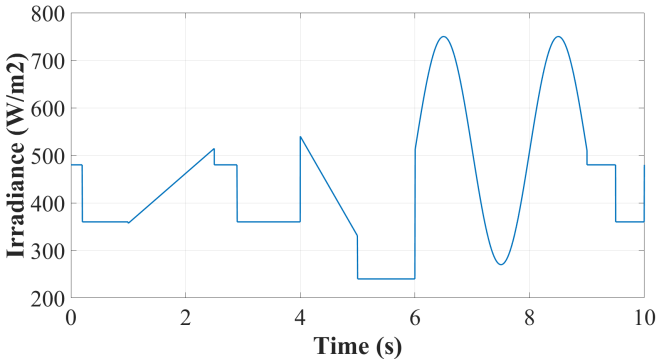

Fig. 5: Irradiance curve for efficiency comparison

TABLE IV: Noise tolerance results for MPPT algorithms

Algorithm	SNR Voltage (dB)	SNR Current (dB)
proposed	33 dB	18 dB
ANN + SCT	34 dB	23dB
PIλ + SCT	40 dB	31dB
SCT	36 dB	23 dB
FLC	42 dB	26dB

C. Results

Fig 3 illustrates the tracking accuracy of the proposed algorithm as compared to modern equivalents. Fig 4 shows the efficiency curves of the proposed algorithm under no noise and critical noise conditions, demonstrating its robustness. Table III and table IV compares the proposed system to other state-of-the-art hybrid and individual algorithms, showing its superior performance across all metrics. Table V summarises the key performance metrics of the proposed algorithm.

VII. Conclusion

The split resistor-based synergetic MPPT algorithm stands out as the most effective MPPT strategy for HALE UAVs. The primary benifits:

- Swift convergence to the maximum power point, even amidst rapidly fluctuating irradiance.
- Exceptional tracking accuracy, maintaining a steady-state error consistently under 0.1%.
- Achieved nearly 99% efficiency across various operating scenarios.
- Exhibits robust noise resilience, ensuring dependable performance even at 18 dB SNR.

Considering practical aerospace constraints like weight, power, and robustness, the FLC + SCT hybrid emerges as a highly deployable and comprehensive MPPT solution for solar-powered HALE UAV systems.

VIII. Future Work

Future work will focus on implementing the proposed MPPT algorithm on embedded hardware to evaluate real-time performance. Adaptive tuning methods, such as machine learning-based optimisation of synergetic parameters, may further enhance tracking under dynamic conditions. Additional efforts will explore integration with UAV flight control, robustness under extreme noise/temperature, and long-duration simulations or flight trials to assess real-world energy gains and mission endurance.

TABLE V: Results of proposed algorithm

System Parameter	Value
Efficiency	98.94%
Convergence time (s)	0.021 s
Steady State Error (%)	$\pm$0.087%
Noise Tolerance	upto 18dB SNR

References

[1] S. Alnaser and A. Omer, "Photovoltaic energy harvesting for aerospace applications: Challenges and opportunities," *Energy Reports*, vol. 7, pp. 1174–1188, 2021.

[2] H. Wang, Y. Liu, and L. Zhao, "High-efficiency mppt strategies for solar-powered uavs under dynamic irradiance," *Journal of Power Electronics*, vol. 22, no. 5, pp. 1001–1013, 2022.

[3] J. Liang, K. Xu, and Y. Zhang, "Advances in high-altitude long endurance (hale) uavs: Energy management and photovoltaic system integration," *IEEE Access*, vol. 11, pp. 15 245–15 260, 2023.

[4] J. Ahmed and Z. Salam, "A comprehensive review of maximum power point tracking algorithms for photovoltaic systems," *Renewable and Sustainable Energy Reviews*, vol. 74, pp. 1142–1158, 2020.

[5] C. Zhang, J. Wang, and H. Liu, "Improved incremental conductance mppt algorithm for solar uavs under dynamic conditions," *International Journal of Photoenergy*, vol. 2021, pp. 1–12, 2021.

[6] M. Y. Allani, D. Mezghani, F. Tadeo, and A. Mami, "Fpga implementation of a robust mppt of a photovoltaic system using a fuzzy logic controller based on incremental and conductance algorithm," *Engineering, Technology & Applied Science Research*, vol. 9, no. 4, pp. 4322–4328, 2019.

[7] Y. Zhou, H. Chen, and P. Xu, "Enhanced fuzzy logic mppt algorithm for solar pv systems in dynamic weather," *Energy Conversion and Management*, vol. 251, p. 114965, 2022.

[8] A. Demirci, I. Dagal, S. Mirza Tercan, H. Gundogdu, M. Terkes, and U. Cali, "Enhanced ann-based mppt for photovoltaic systems: Integrating metaheuristic and analytical algorithms for optimal performance under partial shading," *IEEE Access*, vol. 13, pp. 92 783–92 799, 2025.

[9] P. Chauhan, R. Singh, and S. Yadav, "Artificial intelligence-based mppt algorithms for solar energy harvesting: A review and new perspectives," *Applied Energy*, vol. 336, p. 120857, 2023.

[10] I. Saady, B. Majout, B. Bossoufi, M. Karim, I. Elkafazi, S. Merzouk, M. M. Almalki, T. A. Alghamdi, P. Skruch, A. Zhilenkov *et al.*, "Improving photovoltaic water pumping system performance with pso-based mppt and pso-based direct torque control using real-time simulation," *Scientific Reports*, vol. 15, no. 1, p. 16127, 2025.

[11] R. Sharma, P. Gupta, and V. Singh, "Hybrid intelligent mppt algorithms for photovoltaic systems: A review and future prospects," *Journal of Cleaner Production*, vol. 340, p. 130744, 2022.

[12] K. Xia, Y. Li, and B. Zhu, "Improved photovoltaic mppt algorithm based on ant colony optimization and fuzzy logic under conditions of partial shading," *IEEE Access*, vol. 12, pp. 44 817–44 825, 2024.

[13] O. Saleem, S. Ali, and J. Iqbal, "Robust mppt control of stand-alone photovoltaic systems via adaptive self-adjusting fractional order pid controller," *Energies*, vol. 16, no. 13, p. 5039, 2023.

[14] A. Rawat, S. Jha, B. Kumar, and V. Mohan, "Nonlinear fractional order pid controller for tracking maximum power in photo-voltaic system," *Journal of Intelligent & Fuzzy Systems*, vol. 38, no. 5, pp. 6703–6713, 2020.

[15] A.-B. A. Al-Hussein, F. R. Tahir, and V.-T. Pham, "Fpga implementation of synergetic controller-based mppt algorithm for a standalone pv system," *Computation*, vol. 13, no. 3, p. 64, 2025.

[16] R. Ayat, A. Bouafia, and J.-P. Gaubert, "Experimental validation of synergetic approach based mppt controller for an autonomous pv system," *IET Renewable Power Generation*, vol. 15, no. 7, pp. 1515–1527, 2021.

[17] K. Bharath, P. Venkatesh, and S. Kumar, "Synergetic control-based mppt for photovoltaic systems under dynamic irradiance," *ISA Transactions*, vol. 112, pp. 102–114, 2021.
[18] B. M. Bellah, B. Tahar, and B. Adel, "Adaptive hybrid mppt using artificial intelligence for an autonomous pv system," *International Journal of Smart Grid-ijSmartGrid*, vol. 8, no. 1, pp. 27–34, 2024.
[19] R. Bisht, A. Sikander, A. Sharma, K. Abidi, M. R. Saifuddin, and S. S. Lee, "A new hybrid framework for the mppt of solar pv systems under partial shaded scenarios," *Sustainability*, vol. 17, no. 12, p. 5285, 2025.
[20] L. Chen and X. Wang, "An enhanced mppt method based on ann-assisted sequential monte carlo and quickest change detection," *arXiv preprint arXiv:1805.04922*, 2018.